Interactions of Fluorophores with Iron Nanoparticles: Metal-Enhanced Fluorescence

Yongxia Zhang,[†] Apala Padhyay,[†] Jesus E. Sevilleja,[‡] Richard L. Guerrant,[‡] and Chris D. Geddes*,[§]

Institute of Fluorescence, University of Maryland Baltimore County, 701 East Pratt Street, Baltimore, Maryland 21202, Infectious Diseases for Global Health, University of Virginia School of Medicine, Charlottesville, Virginia 22908, and Institute of Fluorescence and Department of Chemistry and Biochemistry, University of Maryland Baltimore County, 701 East Pratt Street, Baltimore, Maryland 21202

Received: October 21, 2009; Revised Manuscript Received: March 30, 2010

Different density iron nanoparticulate substrates were fabricated by thermal vapor deposition in order to study the interactions of fluorophores with iron nanoparticles. We observed metal-enhanced fluorescence (MEF), when fluorophores were placed in close proximity, in the near-field, to the iron nanoparticle deposited substrates. There is often a strong net absorption effect caused by the localized enhanced electromagnetic field of the incident excitation field, when the luminophore is placed near the metal. Subsequently,the electromagnetic field distributions around different size Fe nanoparticles were simulated using FDTD, which revealed that the maximum electric field intensity is predicted to occur over the ~400−550 nm wavelength range. In addition, the decay time of fluorophores was also reduced near the iron substrates, suggesting both an enhanced electric field and a plasmon-coupling component are the mechanisms for fluorescence enhancement, consistent with our laboratory's current interpretation of MEF.

Introduction

In the last two decades, iron nanoparticles have been increasingly exploited for efficient gene delivery,[1] magnetic resonance imaging (MRI) contrast agents,[2] and mediators of hyperthermia cancer treatment.[3,4] With the development of iron nanoparticles as nanorelated pharmaceutical agents, detailed analysis of pharmacokinetics such as distribution, metabolism, absorption, and excretion is needed to understand the effect of nanoparticles in the body. Typically, in order to trace nanoparticles in the body, they have been conjugated with fluorophores and detected by using imaging technologies. However, in these reports, workers have assumed the fluorescence signal originated solely from the far-field. In recent years, our laboratory has studied the interactions of fluorophores with metallic nanoparticles and developed a mechanism for metal-enhanced fluorescence (MEF),[5−9] whereby metallic nanostructures favorably modify the spectral properties of fluorophores, and alleviate some of their more classical photophysical constraints,[5,8,9] such as low quantum yield and poor photostability. Our current explanation of plasmon−lumophore interactions is subtly different than our own early reports,[5] where it was postulated that it was the fluorophore itself that radiated, its photophysical properties thought to be modified by a resonance interaction with the close proximity to surface plasmons. Our laboratory's current mechanistic interpretation of MEF is underpinned by a model whereby nonradiative energy transfer occurs from excited distal fluorophores to surface plasmons in noncontinuous films (Table 1, right), in essence a fluorophore induced mirror dipole in the metal. The surface plasmons, *in turn*, radiate the photophysical characteristics of the coupling fluorophores. In essence, the *system radiates* as a whole. As a result, the *system* exhibits modified overall radiative rates, in contrast to the

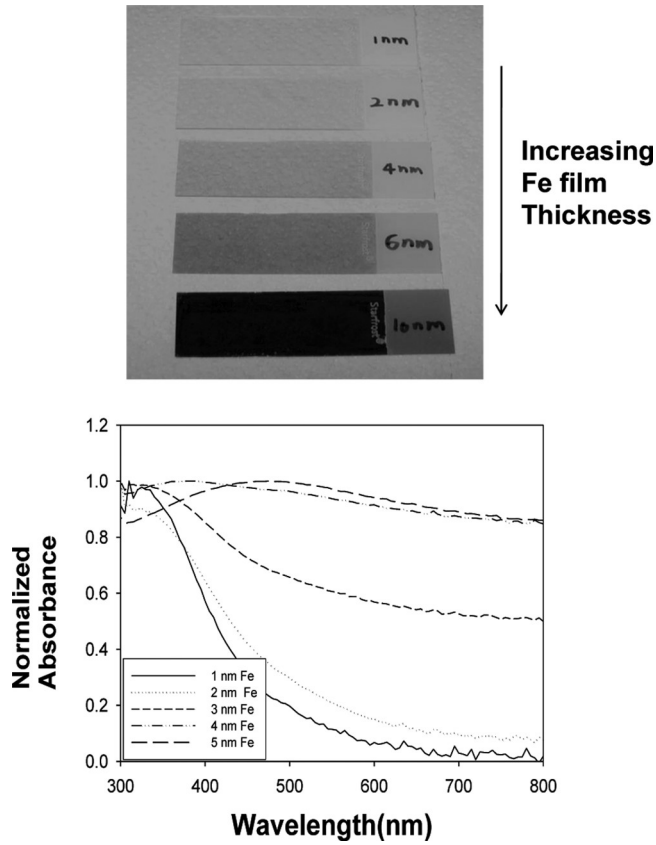

Figure 1. Photograph of glass and Fe slides with different thicknesses of 1, 2, 4, 6, and 10 nm (top), demonstrating the semitransparent nature of the Fe films. Normalized absorption spectrum of vapor deposited metallic Fe of various thicknesses deposited onto glass slides (bottom).

* To whom correspondence should be addressed. Phone: +1-410-576-5723. Fax: +1-410-576-5722. E-mail: geddes@umbc.edu.
[†] Institute of Fluorescence, University of Maryland Baltimore County.
[‡] University of Virginia School of Medicine.
[§] Institute of Fluorescence and Department of Chemistry and Biochemistry, University of Maryland Baltimore County.

10.1021/jp910080b
Published on Web 04/13/2010

TABLE 1: Fluorescence Lifetime of Fluorescein in Water (pH 7.0) and on Fe Nanodeposits Measured Using Time-Domain Fluorometry[a]

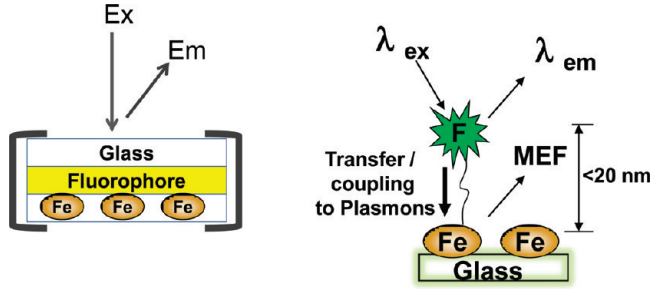

	τ (ns)	A_1 (%)	τ (ns)	A_2 (%)	$\langle\tau\rangle$ (ns)	$\bar{\tau}$ (ns)	χ^2
fluorescein in H_2O in cuvette	3.9	100			3.9	3.9	1.0
fluorescein glass/glass sandwich	3.5	78.9	7.6	21.1	3.9	4.1	1.2
fluorescein 1 nm Fe/glass	0.2	94.7	0.79	5.28	0.2	0.3	1.0
fluorescein 2 nm Fe/glass	0.2	97.3	3.14	2.65	0.3	1.1	1.3
fluorescein 4 nm Fe/glass	0.2	72.1	3.5	27.9	1.0	3.0	1.0

[a] $\langle\tau\rangle$: the amplitude-weighted lifetime. τ: the mean lifetime. The experimental geometry of samples (top left) and schematic representation of our current interpretation of metal-enhanced fluorescence (top right).

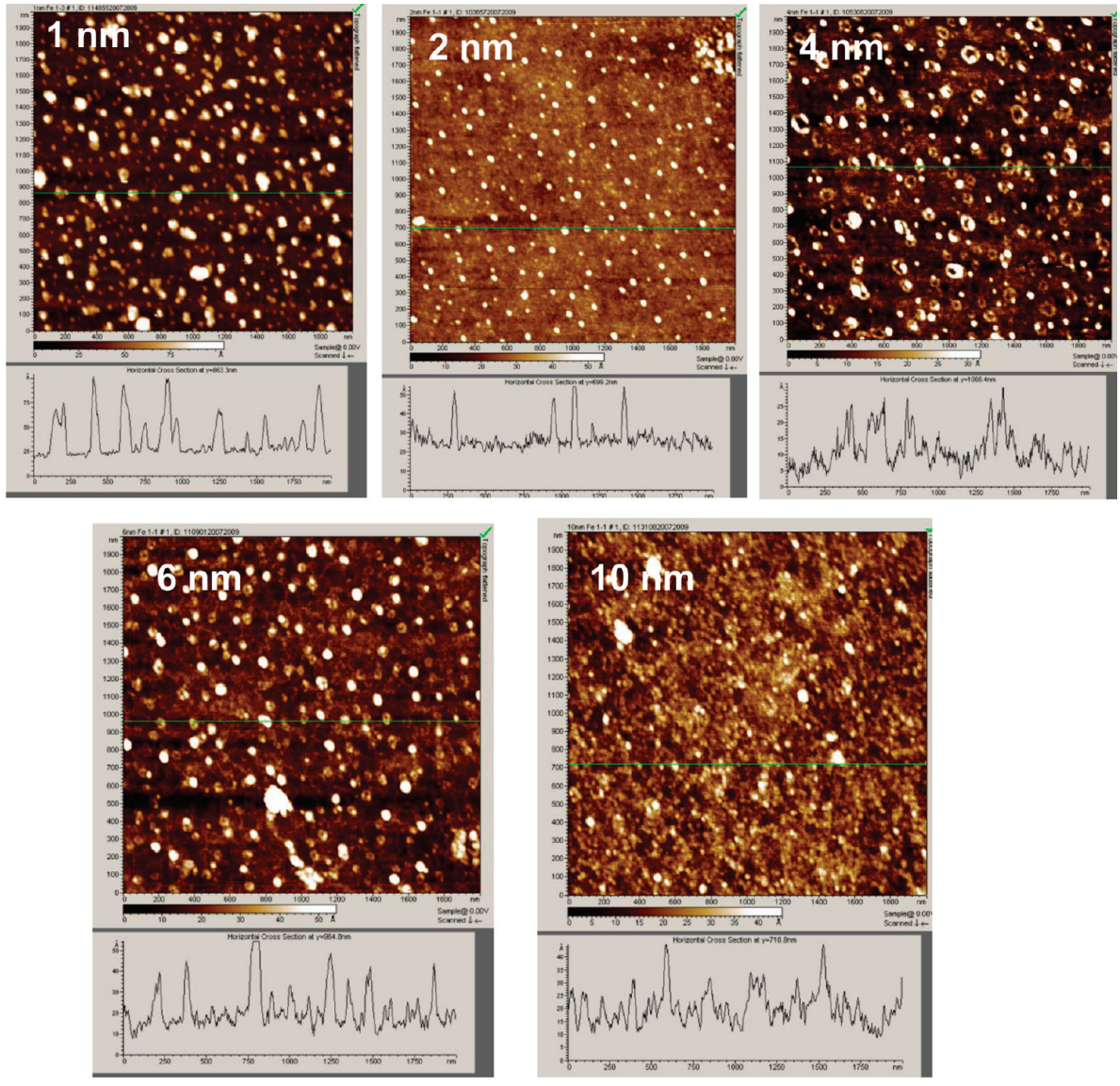

Figure 2. AFM images of 1, 2, 4, 6, and 10 nm Fe on glass. Below are the respective line scans for the AFM images.

fluorophore itself whose rate is thought to be unchanged. Ultimately, the increased radiative rate for the system lends itself to enhanced fluorescence signals or (increased system quantum yields) for fluorophores in close proximity to metallic structures,

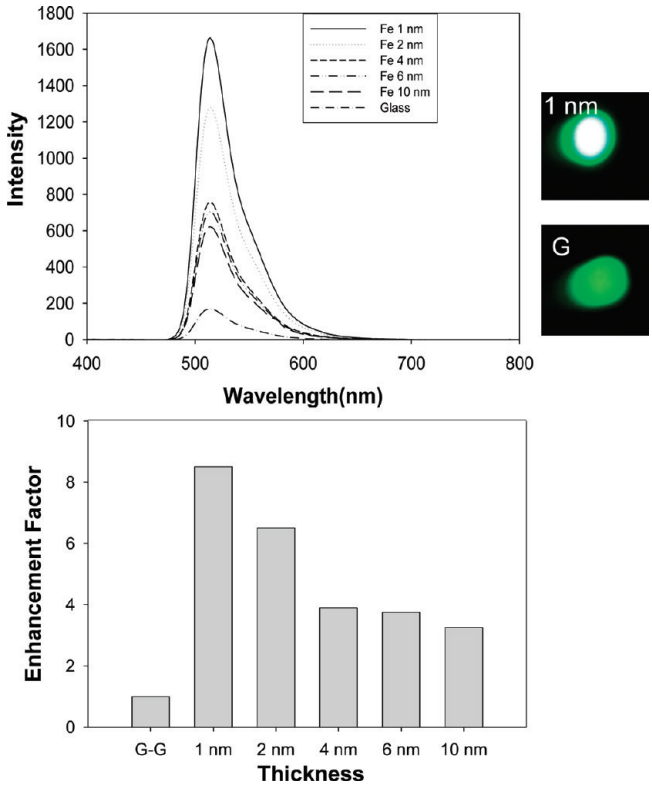

Figure 3. Emission spectra (top) and fluorescence enhancement factor (bottom) for a solution of fluorescein in water sandwiched between glass and Fe slides of varying thicknesses. The enhancement factors were determined from several measurements on the film surface. G-G: Glass sandwich control sample.

which we have shown can be roughly approximated by the following equations:

$$Q_m = (\Gamma + \Gamma_m)/(\Gamma + \Gamma_m + k_{nr}) \quad (1)$$

where Γ is the unmodified *system* radiative decay rate, Γ_m is the metal-modified system radiative decay rate, and k_{nr} are the nonradiative decay rates which are thought for the most part to be unchanged. The metal-modified lifetime, τ_m, of a fluorophore−metal system is also decreased by the increased system radiative decay rate according to the equation

$$\tau_m = 1/(\Gamma + \Gamma_m + k_{nr}) \quad (2)$$

These rate equations are extensions of classical far-field fluorescence expressions, and are only *loosely* thought to approximate the fluorophore−metal coupled system. K_{nr} is assumed to be unaffected by the metal.

MEF is thought to be comprised of two mechanisms: first, an electric field effect, and second, an induced plasmon effect. The enhanced electric field effectively results in an increase in the fluorophore's absorption cross section when in close proximity (<20 nm) to a metal nanoparticle. The second mechanism, the induced plasmon effect, is thought to be based on the partial coupling of excited states of the fluorophores to surface plasmons on the metal nanoparticles (coupled quanta), the nanoparticle radiating the emission, the coupled system lifetime tracking that of the plasmon decay itself.

To date, MEF from many plasmonic nanostructured materials such as silver,[10−13] gold,[14] copper,[15] zinc,[16] chromium,[17] tin,[18]

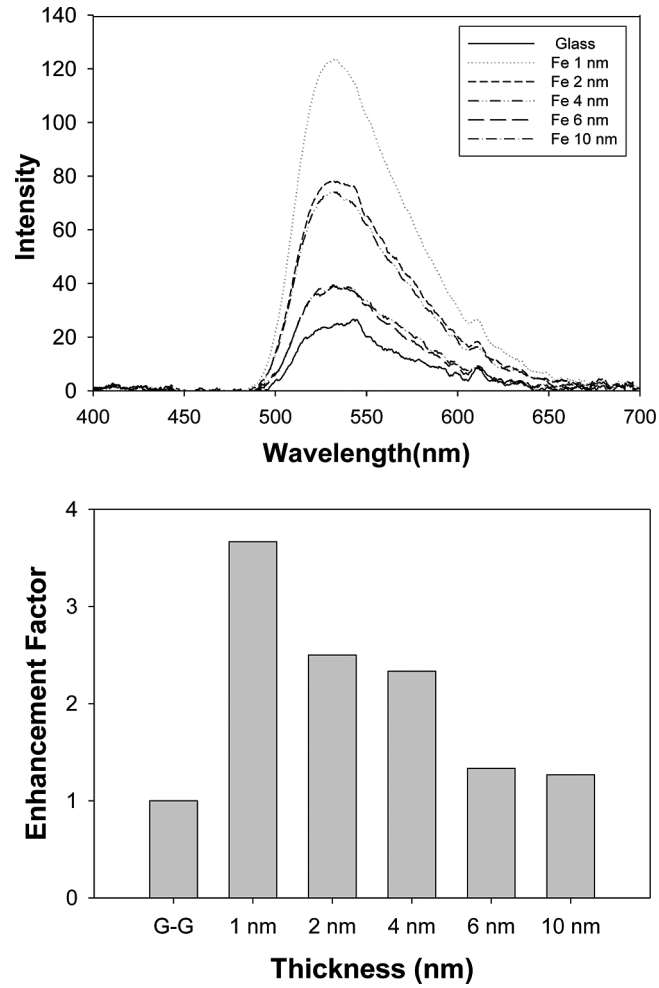

Figure 4. Emission spectra (top) and fluorescence enhancement factor (bottom) for a solution of acridine orange in water sandwiched between glass and Fe slides of varying thicknesses. Ex: 473 nm. The enhancement factors were determined from several measurements on the film surface. G-G: Glass sandwich control sample.

and nickel[19] has been observed by our lab. In this regard, silver, gold, and copper nanoparticles were used for applications of MEF with fluorophores emitting in the visible wavelength region; zinc and chromium nanostructured films were shown to additionally enhance the fluorescence emission of fluorophores in the UV and blue spectral regions, whereas nickel was shown to enhance in the near IR spectral range. In this paper, we subsequently show that magnetic Fe nanoparticle films can also be used for MEF applications. Fe nanodeposits of various thicknesses were deposited, using thermal vapor deposition, onto glass microscope slides, and were characterized by optical absorption and atomic force microscopy (AFM) techniques. Two fluorophores (fluorescein and acridine orange) were deposited onto Fe substrates in a sandwich sample format (Table 1, top right), respectively. Enhancements of fluorescence emission from the fluorophores were both observed and compared. In addition, we have observed a shorter fluorescence lifetime (decay time) for fluorophores in close proximity to Fe nanostructures, which is in complete agreement with other reports and trends for metal-enhanced fluorescence[7,20] and eq 2, which approximates the coupled system lifetime, suggesting that both an enhanced electric field and a plasmon-coupling component underpin the mechanism for fluorescence enhancement, similar to substrates made from silver, copper, and gold nanoparticles.[10,15,21]

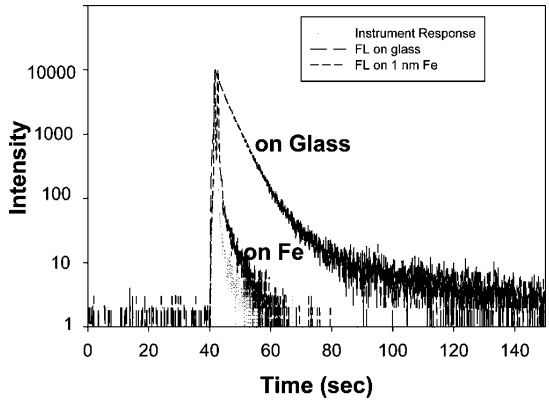

Figure 5. Fluorescence intensity decays of fluorescein from glass−glass and Fe−glass slides.

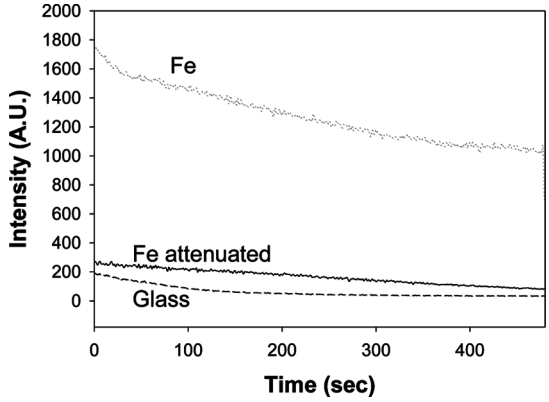

Figure 6. Emission intensity vs time (photostability) of fluorescein on 1 nm Fe films and glass, and with the laper power adjusted to give the same initial steady-state fluorescence intensity on Fe.

Experimental Section

Materials. Fluorophores (fluorescein and acridine orange) were obtained from Sigma-Aldrich Chemical company and used as received. Silane prep glass microscope slides were purchased from Sigma-Aldrich. Iron nanostructured films of various thicknesses were deposited onto silane prep glass microscope slides using thermal vapor deposition, AccuCoat, Inc., Rochester, NY.

Preparation of Sandwich Format Samples for Metal-Enhanced Fluorescence Measurements. A solution of 150 μL of fluorophore (500 nM) was sandwiched between two glass slides for the control sample and between one glass and one iron nanostructured film. The dye was excited with a 473 nm laser line source, and the fluorescence emission spectra were collected after passing through a 473 nm notch filter.

Optical Spectroscopy. The absorption spectra of the iron nanostructured films of varying thicknesses were collected using a Varian Cary 50 UV−vis spectrophotometer. Fluorescence spectra of the fluorophores were measured with blank glass sandwiches and glass-nanostructured film sandwiches using an Ocean Optics HD2000 fluorometer.

Time-Domain Lifetime Measurements. Time-domain lifetime measurements of the fluorophores were measured in a cuvette (solution), glass slide sandwiches, and glass−iron substrate sandwiches in a front-face geometry using a Horiba Jobin Yvon TemPro system with pulsed laser diodes for excitation, a filter, and a TBX4 module for emission. The data was fitted to one and multiexponential decay kinetics using impulse reconvolution analysis and a χ^2 goodness of fit criterion.

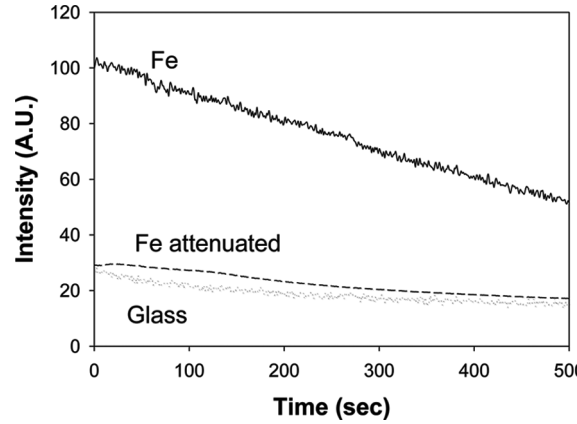

Figure 7. Emission intensity vs time (photostability) of acridine orange on 1 nm Fe films and glass and with the laser power adjusted to give the same initial steady-state fluorescence intensity.

Atomic Force Microscopy (AFM). AFM images were performed on a Molecular Imaging Picoplus Microscope. Samples were imaged at a scan rate of 1 Hz with 512 × 512 pixel resolution in the tapping mode.

FDTD Calculations. The FDTD method was employed to determine the relative electric field intensities and distributions at the surface of iron nanoparticles in a total field scattered field (TFSF), recalling that an enhanced e-field is one of the two mechanisms thought to contribute to fluorescence enhancement. TFSF sources are used to divide the computation area or volume into total field (incident plus scattered field) and scattered field only regions.[22,23] The incident p-polarized electric field is defined as a plane wave with a wavevector that is normal to the injection surface (denoted by the white arrow in Figure 8). The scattered and total fields were monitored during the simulation such that the total or scattered transmission can be measured. Using Lumerical FDTD Solution software, the simulation region is set to 600 × 600 nm with a mesh accuracy of 5. The overall simulation time was set to 200 ns and calculated over a wavelength range from 300 to 800 nm for the iron nanoparticles of different sizes (20−100 nm).

Results and Discussion

The top of Figure 1 shows the respective photographs of different thickness iron slides, allowing one to see their transparency as a function of decreased loading. The bottom of Figure 1 shows the normalized absorption spectra of 1, 2, 4, 6, and 10 nm thick iron films. Iron nanodeposits of 1, 2, and 4 nm show an absorbance peak around 350 nm, suggesting a particulate film. With increasing thickness, a broad flat absorption spectrum was observed, which is indicative of the aggregation and plasmon coupling of the nanodeposits on the surface, typical characteristics of continuous film. These results correlate well with our AFM results. AFM images of 1, 2, 4, 6, and 10 nm iron films are shown in Figure 2. For the 1 nm iron film, we observe separated islands with the height of the islands being ~5 nm, as seen from the line scan results. However, for the 10 nm Fe film, the height of the most separated islands was around 1 nm, which was much lower than the thickness of the iron film measured by the quartz crystal microbalance (QCM) in the thermal evaporator. It can be concluded from the AFM images that, for 1 nm iron samples, only one layer of separated iron islands (similar to separated iron nanoparticles) was formed on the glass slides due to the height of the islands being close to the iron film thickness measured by the QCM. By increasing

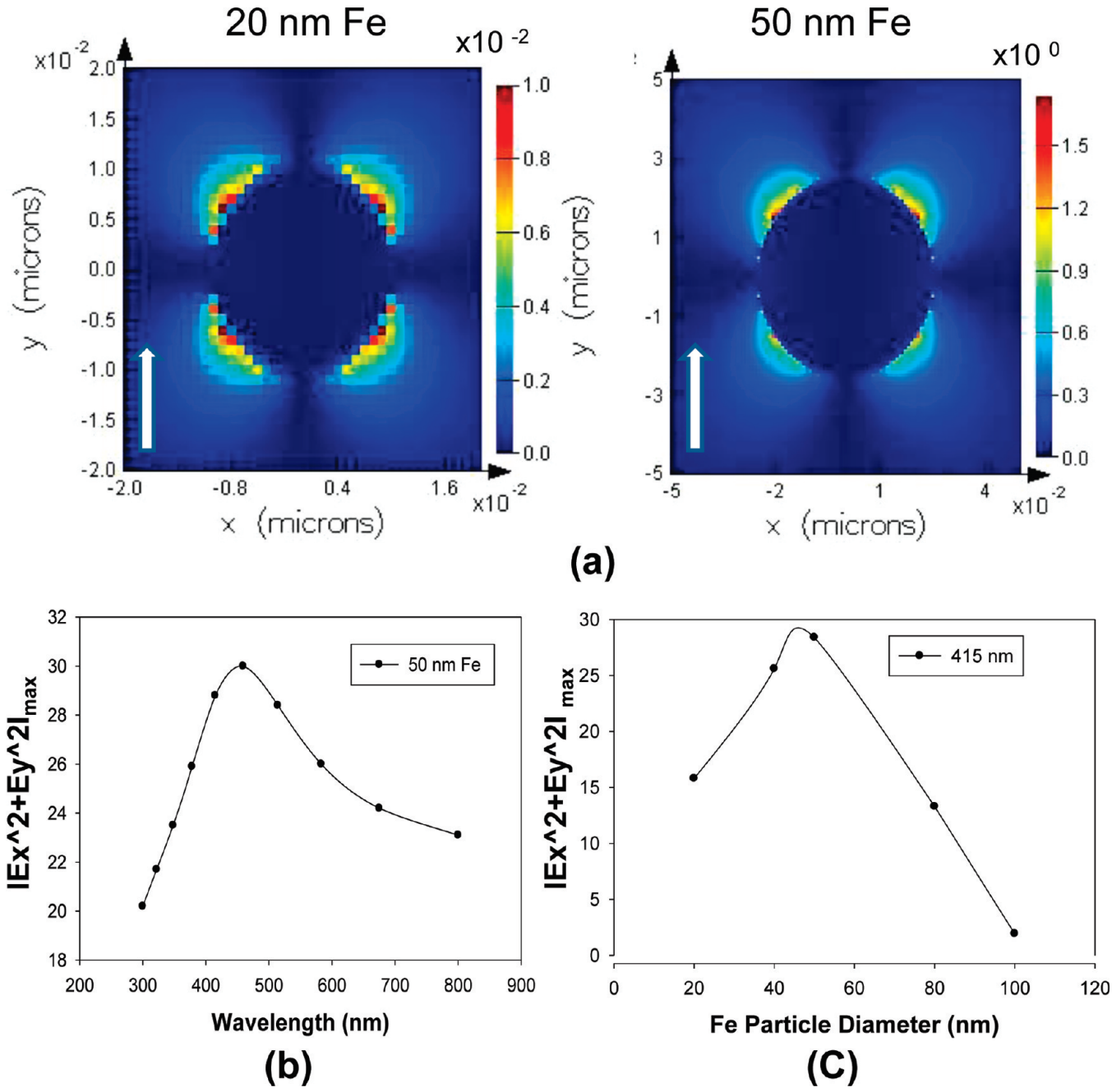

Figure 8. (a) Images of near-field intensity (Ey) distributions around 20 and 50 nm Fe nanoparticles. The white arrow shows the direction of the incident light injection at 415 nm. (b) The dependence of electric field $|Ex^2 + Ey^2|$ maximum intensity upon wavelength of incident light for 50 nm diameter nanoparticles. (c) The dependence of electric field $|Ex^2 + Ey^2|$ maximum intensity upon nanoparticle size with 415 nm incident light injection. Calculations were undertaken using FDTD.

the iron film thickness, iron islands eventually form a continuous film on the glass slide, with the top layer covered by separated iron islands.

The fluorescence emission spectra of fluorescein on different thickness Fe films and on glass are shown in Figure 3. It can be seen that the fluorescence of fluorescein is enhanced (9-fold) for 1 nm Fe, as compared to the glass control sample, i.e., no metal, with the enhancement factor decreased with increased Fe thickness. It is somewhat easy to understand this trend where the enhancement factor is decreased with increased Fe thickness. This finding is consistent with trends observed for continuous and particulate silver[5] and gold films[21] and their influence on MEF, suggesting again that continuous films are poor enhancers of near-filed fluorescence.[21] In this regard, it should be noted that the true metal-enhanced fluorescence enhancement factor is much larger than 9, and is ~450-fold. This is because the MEF phenomenon is through-space with an interaction distance of less than 20 nm. With a sample thickness of 1 μm, then only 2% of the sample is within the MEF enhancement region; hence, the true enhancement factor is approximately 50 times larger.[5] This suggests the near-field enhanced fluorescence is ~450-fold brighter. Considering the nature of Fe, it is thought that a few of the Fe nanoparticles on the top of films might have been oxidized during the measurement. Subsequently, we expect that the enhancement factor might be potentially larger than this estimated near-field value.

In addition, the fluorescence emissions of acridine orange on different thickness Fe films and on glass (control sample) were

investigated, as shown in Figure 4. It can be seen that the fluorescence of acridine orange is enhanced (3.8-fold) on 1 nm Fe, as compared to the glass control sample, i.e., no metal, with a similar trend in enhancement factor as observed with fluoroscein with increased Fe thickness. The enhancement factor for acridine orange is different from that measured for fluorescein. This finding suggests MEF is both wavelength and quantum yield dependent (the emission peak of acridine orange is ~540 nm; the emission peak of fluorescein is ~513 nm) similar to that reported for silver nanoparticles.[24]

The shorter lifetime observed for fluorophores in proximity to metallic nanoparticles has been reported several times before, which is thought to be indicative of the plasmon lifetime itself,[25] recalling that the coupled fluorophore quanta is radiated from the nanoparticles[25] in the model described by Geddes and co-workers.[24,25] In this regard, the lifetimes of fluorescein and acridine orange near iron substrates were measured. The experimental geometry and the overall results of the lifetime analysis are given in Table 1. The decay curve of fluorescence between glass−glass and between glass and 1 nm Fe are shown in Figure 5. The fluorescence decays faster on a 1 nm Fe film than on glass. The decay curve was fitted to one and also multiexponential decay kinetic functions with impulse reconvolution analysis and a χ^2 goodness of fit criterion. The lifetime of fluorescein on glass substrates (sandwich format: glass/fluorescein/glass) is very similar to that for fluorescein in a cuvette (the amplitude-weighted lifetime of fluorescein in bulk solution in a cuvette is 3.9 and 3.9 ns on glass slides) as expected. The amplitude-weighted lifetimes of fluorescein on 1, 2, and 4 nm Fe glass are 0.2, 0.3, and 1.0 ns, respectively. Subsequently, we observed that the lifetime of the fluorophore−metal system is reduced, as expected, due to a faster and more efficient fluorophore−plasmon emission, consistent with eq 2 and our laboratory's current interpretation of the MEF phenomenon.[24,25]

Photobleaching and phototransformation of fluorophores is a widespread problem in the applications of fluorescence where rapid photobleaching occurs for most probes in fluorescent microscopy. In this regard, we have investigated the interactions of metals, such as Ag, Au, Ni, and Sn particles with fluorophores, to increase the fluorophore photostability in the past. Figure 6 shows fluorescein emission as a function of time, excited at 473 nm and observed using a 473 nm notch filter. The relative intensities of the plots reflects that more detectable photons can be observed per unit time from the 1 nm Fe film, as compared to glass (a control sample), where the integrated areas under the plots are proportional to the photon flux from the respective samples. By additionally adjusting the laser power (using a neutral density filter) to match the initial steady-state intensities of the samples, the fluorescein on Fe can be seen to be slightly more photostable. This finding is consistent with the fact that the lifetime of the fluorescein is shorter on a 1 nm Fe film than on glass, the fluorescein molecules in essence spending less time on average in an excited state, due to the fast nonradiative energy transfer to the Fe, and therefore, they are less prone to photodestruction, i.e., are more photostable. The photostability of acridine orange was also measured, as shown in Figure 7. It was also shown that acridine orange is more photostable on 1 nm Fe than on glass, supporting the notion that iron nanoparticles can be used in MEF applications.

Over several years, the Geddes group has proposed two complementary and cumulative effects for the fluorescence enhancement for fluophores in close proximity to metallic nanoparticles:[24,25] (i) surface plasmons can radiate coupled fluorescence efficiently, which contributes to the shorter lifetime (enhanced photostability), and (ii) an enhanced absorption or electric field facilitates enhanced emission. In this regard, we have simulated the electromagnetic field around different size Fe nanoparticles to understand the spatial distributions of the fields using FDTD calculations (Figure 8). Using Lumerical (Canada) FDTD Solution software, the experimental simulation region was set to 600 × 600 nm with a mesh accuracy of 5. The overall simulation time was set to 200 ns and calculated over a wavelength range of 300−800 nm for Fe nanoparticles. For different metallic films made by vapor thermal deposition, the particles are growing in different ways, such as Ag and Sn[18] are growing into different sizes of nanoparticles with increasing film thickness. However, some metals such as Cu[15] nanoparticles are not changing particle size and just growing by layer growth. In this paper, we have chosen 20, 40, 60, 80, and 100 nm diameter particles to show the trends as a function of size at a maximum wavelength of 415 nm, as shown in Figure 8, bottom right. It is shown that a 50 nm Fe nanoparticle has maximum electric field intensity. For Fe, FDTD calculations revealed that the maximum electric field intensity is predicted to occur over a range of wavelengths in the ~400−550 nm range. This suggests that Fe nanoparticles will enhance fluorescence signatures well over this wavelength range.

Conclusions

In this paper, we have studied the effects of iron nanoparticles on near-field fluorescence. We conclude that iron nanoparticles can enhance the intensity of the studied fluorophores. In addition, fluorophores with different emission wavelength maxima and free-space quantum yields in close proximity to iron nanoparticles can undergo different enhanced fluorescence; a 3.8-fold increase was observed from 1 nm Fe films from acridine orange, and up to a 9-fold far-field enhancement was observed for fluorescein (i.e., >1 λ away). In the near-field, fluorescence enhancement values were ~190- and 450-fold, respectively. Furthermore, the decay times of fluorophores were also reduced *near* the Fe substrates, suggesting both an enhanced electric field and a plasmon-coupling component is the mechanism for fluorescence enhancement, similar to substrates made from silver, copper, and gold nanoparticles.

Acknowledgment. The authors acknowledge UMBI and the IoF for salary support. The authors also acknowledge the MARCE and NIH 2U54 AIO5 7168-O6 for support.

References and Notes

(1) Scherer, F.; Anton, M.; Schillinger, U.; Henkel, J.; Bergemann, C.; Kruger, A.; Gansbacher, B.; Plank, C. *Gene Ther.* **2002**, *9*, 102–109.
(2) Bulte, J. W. M.; Douglas, T.; Witwer, B.; Zhang, S. C.; Strable, E.; Lewis, B. K.; Zywicke, H.; Miller, B.; van Gelderen, P.; Moskowitz, B. M.; Duncan, I. D.; Frank, J. A. *Nat. Biotechnol.* **2001**, *19*, 1141–1147.
(3) Ito, A.; Honda, H.; Kobayashi, T. *Cancer Immunol. Immunother.* **2006**, *55*, 320–328.
(4) Fortin, J. P.; Wilhelm, C.; Servais, J.; Menager, C.; Bacri, J. C.; Gazeau, F. *J. Am. Chem. Soc.* **2007**, *129*, 2628–2635.
(5) Geddes, C. D.; Lakowicz, J. R. *J. Fluoresc.* **2002**, *12*, 121–129.
(6) Aslan, K.; Lakowicz, J. R.; Szmacinski, H.; Geddes, C. D. *J. Fluoresc.* **2004**, *14*, 677–679.
(7) Aslan, K.; Malyn, S. N.; Bector, G.; Geddes, C. D. *Analyst* **2007**, *132*, 1122–1129.
(8) Aslan, K.; Previte, M. J. R.; Zhang, Y. X.; Baillie, L.; Geddes, C. D. *Biophys. J.* **2007**, 552A–552A.
(9) Aslan, K.; Zhang, Y.; Hibbs, S.; Baillie, L.; Previte, M. J.; Geddes, C. D. *Analyst* **2007**, *132*, 1130–1138.
(10) Aslan, K.; Lakowicz, J. R.; Geddes, C. D. *Anal. Bioanal. Chem.* **2005**, *382*, 926–933.
(11) Aslan, K.; Badugu, R.; Lakowicz, J. R.; Geddes, C. D. *J. Fluoresc.* **2005**, *15*, 99–104.

(12) Aslan, K.; Leonenko, Z.; Lakowicz, J. R.; Geddes, C. D. *J. Phys. Chem. B* **2005**, *109*, 3157–3162.
(13) Aslan, K.; Lakowicz, J. R.; Geddes, C. D. *J. Phys. Chem. B* **2005**, *109*, 6247–6251.
(14) Aslan, K.; Lakowicz, J. R.; Geddes, C. D. *Anal. Biochem.* **2004**, *330*, 145–155.
(15) Zhang, Y.; Aslan, K.; Previte, M. J. R.; Geddes, C. D. *Appl. Phys. Lett.* **2007**, *90*, 173116.
(16) Aslan, K.; Previte, M. J. R.; Zhang, Y.; Geddes, C. D. *J. Phys. Chem. C* **2008**, *112*, 18368–18375.
(17) Pribik, R.; Aslan, K.; Zhang, Y.; Geddes, C. D. *J. Phys. Chem. C* **2008**, *112*, 17969–17973.
(18) Zhang, Y.; Dragan, A.; Geddes, C. D. *J. Appl. Phys.*, in press.
(19) Zhang, Y.; Dragan, A.; Geddes, C. D. *J. Phys. Chem. C* **2009**, *113*, 15811–15816.
(20) Geddes, C. D. *J. Fluoresc.*, in press.
(21) Aslan, K.; Malyn, S. N.; Geddes, C. D. *J. Fluoresc.* **2007**, *17*, 7–13.
(22) Taflove, A.; Hagness, S. C. *Computational Electrodynamics: The Finite-Difference Time-Domain Method*, 2nd ed.; Artech House: Norwood, MA, 2000.
(23) Anantha, V.; Taflove, A. *IEEE Trans. Antennas Propag.* **2002**, *50*, 1337–1349.
(24) Zhang, Y.; Dragan, A.; Geddes, C. D. *J. Phys. Chem. C* **2009**, *113*, 12095–12100.
(25) Aslan, K.; Zhang, Y. X.; Geddes, C. D. *J. Appl. Phys.* **2008**, *103*, 084307.

JP910080B